# Effect of Pores Formation Process and Oxygen Plasma Treatment to Hydroxyapatite Formation on Bioactive PEEK Prepared by Incorporation of Precursor of Apatite

Takeshi Yabutsuka[1,*], Keito Fukushima[1], Tomoko Hiruta[1], Shigeomi Takai[1], Takeshi Yao[2]

[1]Department of Fundamental Energy Science, Graduate School of Energy Science, Kyoto University, Yoshida-Honmachi, Sakyo-ku, Kyoto 606-8501, Japan

[2]National Institute of Technology, Kagawa College, 355, Chokushi-cho, Takamatsu, Kagawa 761-8058, Japan

*Corresponding author: Takeshi Yabutsuka

TEL: +81-75-753-9129

FAX: +81-75-753-9115

E-mail: yabutsuka@energy.kyoto-u.ac.jp

**Abstract**

When bioinert substrates with fine-sized pores are immersed in a simulated body fluid (SBF) and the pH value or the temperature is increased, fine particles of calcium phosphate, which the authors denoted as ‘precursor of apatite’ (PrA), are formed in the pores. By this method, hydroxyapatite formation ability can be provided to various kinds of bioinert materials. In this study, the authors studied fabrication methods of bioactive PEEK by using the above-mentioned process. First, the fine-sized pores were formed on the surface of the PEEK substrate by $H_2SO_4$ treatment. Next, to provide hydrophilic property to the PEEK, the surfaces of the PEEK were treated with $O_2$ plasma. Finally, PrA were formed in the pores by the above-mentioned process, which is denoted as ‘Alkaline SBF’ treatment, and the bioactive PEEK was obtained. By immersing in SBF with the physiological condition, hydroxyapatite formation was induced on the whole surface of the substrate within 1 day. The formation of PrA directly contributed to hydroxyapatite formation ability. By applying the $O_2$ plasma treatment, hydroxyapatite formation was uniformly performed on the whole surface of the substrate. The $H_2SO_4$ treatment contributed to a considerable enhancement of adhesive strength of the formed hydroxyapatite layer formed in SBF because of the increase of surface areas of the substrate. As a comparative study, the sandblasting method was applied as the pores formation process instead of the $H_2SO_4$ treatment. Although hydroxyapatite formation was provided also in this case, however, the adhesion of the formed hydroxyapatite layer to the substrate was not sufficient even if the $O_2$ plasma treatment was conducted. This result indicates that the fine-sized pores should be formed on the whole surface of the substrate uniformly to achieve high adhesive strength of the hydroxyapatite layer. Therefore, it is considered that the $H_2SO_4$ treatment before the $O_2$ plasma and the ‘Alkaline SBF’ treatment is an important factor to achieve high adhesive strength of hydroxyapatite layer to the PEEK substrate. This material is expected to be a candidate for next-generation implant materials with high bioactivity.

**Keywords**

PEEK, Bioactivity, Precursor of apatite (PrA), Pores formation, Oxygen plasma treatment

## 1. Introduction

Since the discovery of Bioglass® [1-3], invented by Hench et al., many kinds of bioactive ceramics such as Ceravital® [4], glass-ceramic A-W [5-7], sintered hydroxyapatite ($Ca_{10}(PO_4)_6(OH)_2$) [8-11], etc. have been developed for orthopedic applications. It was reported that many kinds of bioactive ceramics formed hydroxyapatite layer on their surfaces in living body and bond to living bone through this layer [12-14]. This phenomenon is defined as 'bioactivity' among researchers of the ceramic-based biomaterials and is thought to be one of the important material properties of osteoconductive biomaterials. Kokubo et al. reported that the hydroxyapatite formation in living body can be reproduced in a simulated body fluid (SBF) with inorganic ion concentrations nearly equal to those of human blood plasma [15-18]. Hence, it can be predicted that the materials performed hydroxyapatite formation on their surfaces in SBF form hydroxyapatite layer in living body and bond to living bone through this layer.

The bioactive ceramics have been widely used in orthopedic or dental fields for bone substitutes. Although they have high biocompatibility and bioactivity, however, a range of acceptable affected parts is limited because of their mechanical brittleness and low toughness. From the viewpoint of an enhancement of mechanical strength of the bioactive materials, many researchers have studied various kinds of new surface treatments to metals such as titanium and its alloys to provide bioactivity. However, the conventional metals for clinical use have much higher Young's modulus, more than 100 MPa, than that of human cortical bone, ca. 18 GPa [19]. When the metals are used as artificial bones, there is a possibility that a stress shielding phenomenon generated and density of a surrounding living bone decreases [20]. Hence, an establishment of fabrication processes of bioactive materials with low Young's modulus has been desired.

As one of the solution for the above-mentioned problem, organic-inorganic composites have been proposed for clinical applications. Generally, organic polymers are easily processed in various shapes and combined with various kinds of materials such as ceramics. In early 1980s, Bonfield et al. proposed HAPEX™ as an implant material with similar Young's modulus to human cortical bone [21,22]. HAPEX™ was fabricated by dispersing hydroxyapatite powders in high density polyethylene matrix in micro-level. It is reported, however, that this method, mixings of polymeric powders and

ceramics ones, has problems of fractures between organic components and inorganic ones and a low selectivity of materials composition and controls of the fine structure [23].

In a recent decade, polyetheretherketone (PEEK) has attracted much attention as a biomaterial which can be overcoming these physical disadvantages of ceramics and metals in clinical use. PEEK is one of the most attractive super engineering plastic materials with high mechanical properties such as an excellent fatigue, shock, abrasion and chemical resistance. Moreover, its Young's modulus, ca. 4 MPa [19], is similar to that of cortical bone than those of the conventional metallic biomaterials. For these reasons, PEEK has been expected to be a candidate for replacing conventional metal implants and already used as an interbody spacer in orthopedic fields. However, bioactivity of PEEK is extremely low. If the bioactivity is successfully provided to PEEK, an implant material with osteoconductivity as well as good mechanical performance can be developed.

Recently, several kinds of fabrication process for bioactive PEEK has been reported [24]. From a viewpoint of composite formation, PEEK-hydroxyapatite composite [25-27] and PEEK-$CaO{\cdot}SiO_2$ composite [28] have been proposed. However, large amount of the ceramics is needed to add in the PEEK matrix to provide osteoconductivity because only a part of the ceramics is exposed to body fluid to contribute to their bioactivity [29]. From a viewpoint of surface modification, $H_2SO_4$ treatment [30] and $H_2SO_4$ and $CaCl_2$ treatment [29], etc. have been proposed as a bioactivity treatment to PEEK. However, most of the methods require several weeks for formation of hydroxyapatite in SBF. Shimizu et al. suggested that hydroxyapatite formation ability in SBF is the most reliable predictor of osteoconductivity compared with alkaline phosphatase test in their study about bioactive PEEK fabricated by the sol-gel $TiO_2$ coating, which showed hydroxyapatite formation ability within 3 days in SBF [31]. From this point, it is thought that the hydroxyapatite formation ability in SBF is one of the most important factor to predict osteoconductivity. In addition, it was reported that most of bioactive materials for orthopedic application form hydroxyapatite within 1 week [16]. Hence, it is considered that high hydroxyapatite formation ability like in the case of alkali- and heat-treated titanium [32], which showed hydroxyapatite formation within 1 day in SBF, is required also to bioactive PEEK to enhance bone bonding ability in living body.

In a series of our recent reports, the authors presented the production methods of bioactive materials by incorporation of fine particles of calcium phosphate to bioinert materials [33]. When the substrates with fine-sized pores were immersed in SBF and the pH value or the temperature was increased, a homogeneous nucleation of calcium phosphate was promoted and fine particles of amorphous calcium phosphate which act as precursors of apatite [34], defined as 'PrA' in this report, were formed in the pores. By this method, high bioactivity, i.e. hydroxyapatite formation ability, was successfully provided to various kinds of bioinert materials such as metals, ceramics and polymers.

In this study, the authors investigated the fabrication process of bioactive PEEK by incorporation of PrA to PEEK substrates. As a first process, the authors formed fine-sized pores on the surface of the PEEK substrate by $H_2SO_4$ treatment. As a second process, the authors conducted $O_2$ plasma treatment [35] to provide hydrophilic property to the PEEK substrate. As a final process, the authors formed PrA in the pores of the PEEK substrate by the method described above. Bioactivity of thus treated PEEK substrates was evaluated by immersion in SBF with a physiological condition and observation of hydroxyapatite formation on the substrate and adhesive strength of the hydroxyapatite layer formed in the SBF was investigated. Relationships between each treatment and the material properties was considered. As a comparative study, in addition, a sandblasting process was applied as a pores formation process instead of the $H_2SO_4$ treatment and differences on hydroxyapatite formation was considered.

## 2. Materials and Methods

### 2.1. Preparation of SBF

Table 1 shows inorganic ion concentrations of SBF and human blood plasma. SBF was prepared by dissolving reagent-grade NaCl (Wako Pure Chemical Industries, Ltd., Osaka, Japan), $NaHCO_3$ (Hayashi Pure Chemical Ind., Ltd., Osaka, Japan), KCl (Hayashi Pure Chemical Ind., Ltd., Osaka, Japan), $K_2HPO_4 \cdot 3H_2O$ (Nacalai Tesque, Inc., Kyoto, Japan), $MgCl_2 \cdot 6H_2O$ (Hayashi Pure Chemical Ind., Ltd., Osaka, Japan), 1 $mol \cdot dm^{-3}$ HCl (Hayashi Pure Chemical Ind., Ltd., Osaka, Japan), $CaCl_2$ (Hayashi Pure Chemical Ind., Ltd., Osaka, Japan), $Na_2SO_4$ (Hayashi Pure Chemical Ind., Ltd.,

Osaka, Japan) and $(CH_2OH)_3CNH_2$ (Hayashi Pure Chemical Ind., Ltd., Osaka, Japan) in an ultrapure water with a composition as shown in Table 2 in order and adjusted at pH 7.40, 36.5 °C by dissolving 1 mol·dm$^{-3}$ HCl.

Table 1 Inorganic ion concentrations of simulated body fluid (SBF) and human blood plasma [18].

| Ion | Ion concentrations / mmol·dm$^{-3}$ | |
|---|---|---|
| | SBF | Blood plasma |
| $Na^+$ | 142.0 | 142.0 |
| $K^+$ | 5.0 | 5.0 |
| $Mg^{2+}$ | 2.5 | 2.5 |
| $Ca^{2+}$ | 1.5 | 1.5 |
| $Cl^-$ | 147.8 | 103.0 |
| $HCO_3^-$ | 4.2 | 27.0 |
| $HPO_4^{2-}$ | 1.0 | 1.0 |
| $SO_4^{2-}$ | 0.5 | 0.5 |

Table 2 Amounts of dissolved reagents in preparation of 1 dm$^3$ SBF [18].

| Reagent | Amount |
|---|---|
| NaCl | 7.996 g |
| $NaHCO_3$ | 0.350 g |
| KCl | 0.224 g |
| $K_2HPO_4·3H_2O$ | 0.228 g |
| $MgCl_2·6H_2O$ | 0.350 g |
| 1 mol·dm$^{-3}$ HCl | 35 mm$^3$ |
| $CaCl_2$ | 0.278 g |
| $Na_2SO_4$ | 0.071 g |
| $(CH_2OH)_3CNH_2$ | 6.057 g |

**2.2. Substrate**

Commercially obtained PEEK plates (Plaport, Shizuoka, Japan) with 15 mm × 10 mm × 5 mm in size were used as substrates. The PEEK substrates were washed with acetone, ethanol and distilled water by using an ultrasonic cleaner for 10 minutes and air-dried at room temperature. This sample is denoted as ‘Sample N’, hereafter.

### 2.3. Fabrication of bioactive PEEK (Method 1: Employment of $H_2SO_4$ treatment as pores formation)

In this study, the authors applied two kinds of pores formation processes named ‘Method 1’ and ‘Method 2’.

As Method 1, the authors applied $H_2SO_4$ treatment as a pores formation process and bioactive PEEK was fabricated.

#### 2.3.1 Samples preparation

##### 2.3.1.1. $H_2SO_4$ treatment

The surfaces of Sample N were treated with 98 wt% $H_2SO_4$ (Hayashi Pure Chemical Ind., Ltd., Osaka, Japan) for 2 seconds at room temperature twice. Then the substrates were washed in distilled water and air-dried at room temperature. This sample is denoted as ‘Sample S’, hereafter.

##### 2.3.1.2. $O_2$ plasma treatment

To provide hydrophilic properties, surfaces of Sample S was treated with $O_2$ plasma generated by a glow-discharge equipment (Model BP-1, Samco Inc., Kyoto, Japan) using $O_2$ gas (Kyoto Teisan K.K., Kyoto, Japan) at 200 W for 2 minutes. This sample is denoted as ‘Sample SP’, hereafter.

##### 2.3.1.3. ‘Alkaline SBF’ treatment

The pH value of SBF were increased to 8.40 by dissolving $(CH_2OH)_3CNH_2$ at 25.0 °C. This solution is denoted as ‘Alkaline SBF’, hereafter. To precipitate PrA in the pores of the PEEK substrates, Sample SP was immersed in the ‘Alkaline SBF’ and put in an incubator held at 70.0 °C for 24 hours. This sample is denoted as ‘Sample SPA’, hereafter.

##### 2.3.1.4. Combination of each treatment

To investigate which combination of above three treatments ($H_2SO_4$ treatment, $O_2$ treatment, and ‘Alkaline SBF’ treatment) contributes to hydroxyapatite formation ability, seven kinds of samples

shown in Table 3 were prepared by changing combinations of each treatment. In the sample names shown in Table 3, 'S' means that $H_2SO_4$ treatment was conducted, 'P' means that $O_2$ plasma treatment was conducted, 'A' means that 'Alkaline SBF' treatment was conducted, and 'N' means that no treatments were conducted, respectively. In each treatment shown in Table 3, '○' means that the treatment was conducted and '-' means that the treatment was not conducted.

Table 3 List of prepared samples and the combination of each surface treatment in Method 1.

| Procedure | Sample name | $H_2SO_4$ | $O_2$ plasma | 'Alkaline SBF' |
|---|---|---|---|---|
| Before treatment | N | - | - | - |
| 1st treatment | S | ○ | - | - |
| 2nd treatment | SP | ○ | ○ | - |
| 3rd treatment | SPA | ○ | ○ | ○ |
| Reference | A | - | - | ○ |
| Reference | SA | ○ | - | ○ |
| Reference | PA | - | ○ | ○ |

○: conducted.
-: Not conducted.

### 2.3.2. Materials analyses

Changes in functional groups of the surfaces of the substrates were investigated by Fourier transform infrared spectroscopy (FT-IR; FT-720, Horiba, Ltd., Kyoto, Japan) with an attenuated total reflection (ATR) method. Changes in surface morphologies and element compositions of the substrates were analyzed by field emission scanning electron microscopy (FE-SEM; SU6600, Hitachi High-Technologies Corporation, Tokyo, Japan) and energy dispersive X-ray analysis (EDX; XFlash® 5010, Bruker, Germany). Before the FE-SEM and EDX observation, a gold was coated on the substrates by a sputtering method. Changes in crystal phase of the surfaces of the substrates were analyzed by thin film X-ray diffraction (TF-XRD, Rint 2500, Rigaku Corporation, Tokyo, Japan) by using Cu-Kα radiation at 50 kV, 300 mA. Changes in surface area and 3D morphologies of the surface of the substrates were analyzed by ultra-precision point autofocus probe 3D measuring instrument (NH-3SP, Mitaka Kohki Co., Ltd., Tokyo, Japan).

### 2.3.3. Evaluation of hydroxyapatite formation ability

Hydroxyapatite formation ability of each substrate was evaluated by immersion in SBF adjusted

at physiological condition, pH 7.40 at 36.5 °C. After the immersion in SBF for 1 day, 4 days, 7 days and 14 days, the substrates were washed with distilled water and air-dried at room temperature. Changes in functional groups of the surfaces of the substrates were analyzed by FT-IR. Changes in crystal phase of the surfaces of the substrates were analyzed by TF-XRD. Changes in surface morphologies and element compositions of the surfaces of the substrates were analyzed by FE-SEM and EDX.

#### 2.3.4. Measurement of adhesive strength of hydroxyapatite layer formed in SBF

Adhesive strength between the substrates and the hydroxyapatite layer formed by the immersion in SBF for 14 days was investigated by a modified ASTM C-633 method [36-38]. A couple of stainless steel jigs (10 mm × 10 mm) were fixed to both surfaces of the substrates by using Araldite® glue (Huntsman Advanced Materials, USA) and a tensile load was applied at 1 $mm \cdot min^{-1}$ of a crosshead speed until a fracture occurred between hydroxyapatite layers and the substrates by using an universal testing machine (Model AGS-H Autograph, Shimadzu Corporation, Kyoto, Japan).

### 2.4. Fabrication of bioactive PEEK (Method 2: Employment of sandblasting method as pores formation)

As Method 2, the authors applied a sandblasting method as a pores formation process for a comparative study and bioactive PEEK was fabricated.

Table 4 summarizes the prepared samples and the combination of each treatment in Method 2. The surfaces of the PEEK substrates were treated by sandblasting process at 0.85 MPa for discharge pressure for 2 minutes using $Al_2O_3$ grinding particles with 44 μm or 14 μm for average particle size. These samples are denoted as ‘Sample 44’ or ‘Sample 14’, hereafter. In addition, the substrates treated by doubled sandblasting process [39] using the $Al_2O_3$ particles with 44 μm in size for 1 minutes and then 14 μm in size for 1 minutes, denoted as ‘Sample 44-14’ hereafter, were also prepared. The substrates were washed in acetone, ethanol and distilled water by using an ultrasonic cleaner for 10 minutes and air-dried at room temperature.

Next, the surfaces of Sample 44, Sample 14 and Sample 44-14 were treated with $O_2$ plasma at

270 W for 3 minutes. To precipitate PrA in the pores of the substrates, the treated substrates were immersed in the 'Alkaline SBF' and put in an incubator held at 70.0 °C for 24 hours. These substrates are denoted as 'Sample 44PA', 'Sample 14PA' or 'Sample 44-14PA', hereafter.

Hydroxyapatite formation ability of Sample 44PA, Sample 14PA and Sample 44-14PA were evaluated by the immersion in SBF adjusted at pH 7.40, 36.5 °C. After the immersion in SBF for 7 days, the substrates were washed with distilled water and air-dried at room temperature. The surfaces of the substrates were analyzed by FE-SEM and EDX.

Table 4 List of prepared samples and the combination of each surface treatment in Method 2.

| Sample name | 1st Sandblasting (44 μm $Al_2O_3$) | 2nd Sandblasting (14 μm $Al_2O_3$) | $O_2$ plasma | 'Alkaline SBF' |
|---|---|---|---|---|
| 44 | ○ | - | - | - |
| 14 | - | ○ | - | - |
| 44-14 | ○ | ○ | - | - |
| 44PA | ○ | - | ○ | ○ |
| 14PA | - | ○ | ○ | ○ |
| 44-14PA | ○ | ○ | ○ | ○ |

○: conducted.
-: Not conducted.

## 3. Results and Discussion

### 3.1. Method 1： Employment of $H_2SO_4$ treatment as pores formation

#### 3.1.1. PEEK substrates treated by the $H_2SO_4$ and then the $O_2$ plasma

The FE-SEM photograph and the EDX spectrum of the surface of the Sample N, the untreated PEEK substrate, are shown in Figs.1(a) and 1(b). By the FE-SEM observation, a smooth surface was observed on the whole surface of the substrate as shown in Fig.1(a). By the EDX, peaks of C-Kα and O-Kα were observed as shown in Fig.1(b). In addition, a peak of Si-Kα, contained by a preparation process of the PEEK plates, were observed. A peak of Au-Mα derived from the gold coating for the observation was also observed.

The FE-SEM photograph and the EDX spectrum of the surface of the Sample S, the substrate

treated by the $H_2SO_4$, are shown in Figs.1(c) and 1(d). By the FE-SEM observation, it was observed that cancellous pores around ca. 500 nm in diameter were formed on the whole surface of the substrate as shown in Fig.1(c) similar to Zhao's study [30]. In the EDX spectrum, peaks except C-Kα, O-Kα, Si-Kα and Au-Mα were not observed as shown in Fig.1(d). Miyazaki et al. reported that PEEK substrate treated with 97 wt% $H_2SO_4$ at 20 ºC for 10 min were generated a strong peak of S-Kα around 2.3 keV in EDX [29]. However, such peak was not observed in this study. As mentioned in Materials and Methods, the $H_2SO_4$ treatment was conducted in much shorter period, for 4 second in total, in this study. Hence, from the viewpoint of the difference of treatment time, it is considered that sulfurization by the $H_2SO_4$ treatment was less progressed in such short period and peaks of S-Kα was not observed in EDX.

The FE-SEM photograph and the EDX spectrum of the surface of Sample SP, the substrate treated by the $H_2SO_4$ and then the $O_2$ plasma, are shown in Figs.1(e) and 1(f). By FE-SEM observation, the surface morphology was changed from Sample S as shown in Fig.1(e). It is suggested that such morphological change was occurred by heat generated during the $O_2$ plasma treatment. The EDX spectrum was similar to that of Sample S as shown in Fig.1(f).

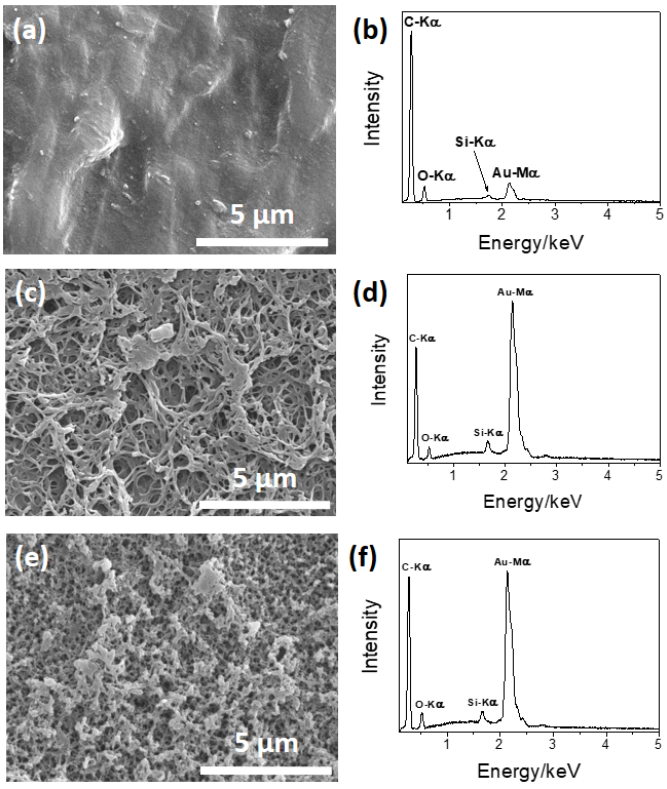


Fig.1 (a,c,e) FE-SEM photographs and (b,d,f) EDX spectra of the surface of (a,b) Sample N, (c,d) Sample S and (e,f) Sample SP.

The 3D images and frequency distribution of the heights on the surfaces of the Sample N, Sample S and Sample SP are shown in Fig.2. After the $H_2SO_4$ treatment, it was observed that a fine rolling was uniformly formed on the surface of the substrate as shown in Fig.2(c). After the $O_2$ plasma treatment, the 3D image was similar to that of Sample S as shown in Fig.2(e). In addition, the heights on each surface was distributed less than 5 μm as shown in Figs.2(b), 2(d) and 2(f). From this result, it was estimated that the fine pores formed by the $H_2SO_4$ treatment possessed the depth of several micron levels.

Zhao et al. reported that porous-structured layer with around 100 μm thickness was formed on the PEEK substrate by treating the substrate with 95-98 wt% $H_2SO_4$ at room temperature for 5 minutes [30]. In our study, the time of $H_2SO_4$ treatment is 4 second in total and much shorter than Zhao's method. Hence, the depth of pores was much smaller and it is possible that the abrasive toughness of the $H_2SO_4$-treated PEEK will be enhanced.

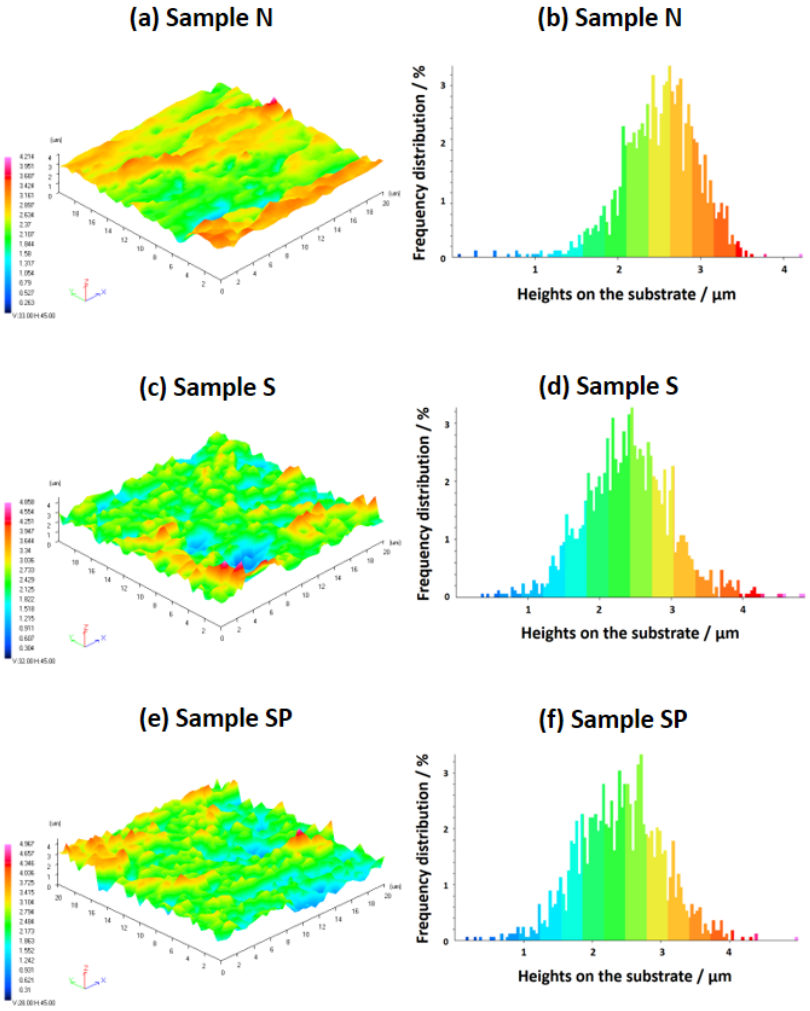


Fig.2 (a,c,e) Three-dimensional images and (b,d,e) frequency distribution of the heights on the surfaces of (a,b) Sample N, (c,d) Sample S and (e,f) Sample SP.

The values obtained by dividing surface areas at the parts shown in Fig.2 by the base area (400 $\mu m^2$) for Sample N, Sample S and Sample SP are summarized in Fig.3. The value was 1.267 for Sample N, 1.637 for Sample S, and 1.717 for Sample SP, respectively. It is indicated that the surface area showed a trend to increase as conducting each stage of the surface treatments.

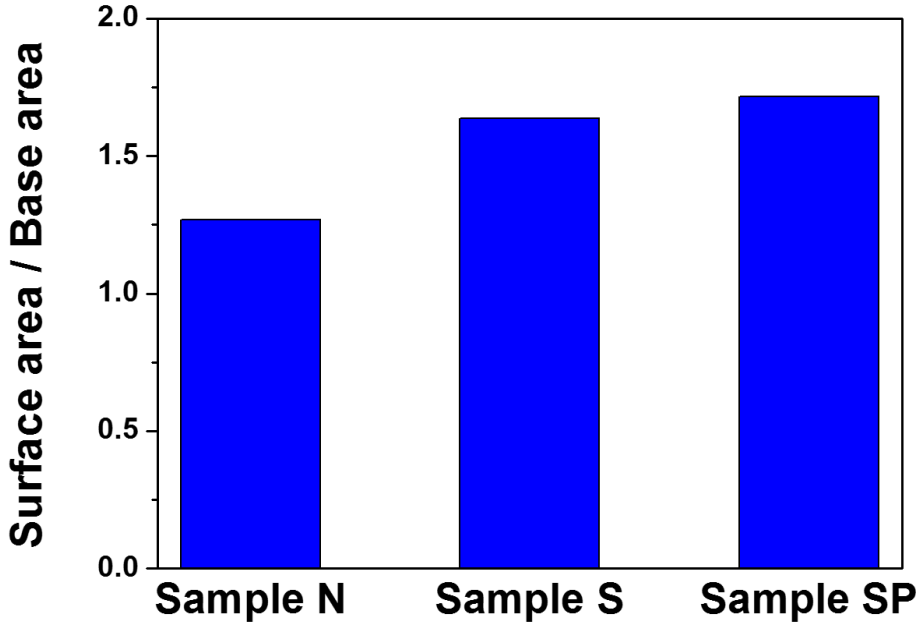


Fig.3 The values obtained by dividing surface areas at the parts shown in Fig.2 by the base area (400 $\mu m^2$) for Sample N, Sample S and Sample SP.

### 3.1.2. PEEK substrates after the 'Alkaline SBF' treatment

The FT-IR spectrum of the surface of the Sample SPA, the substrate treated by the $H_2SO_4$, the $O_2$ plasma and then the 'Alkaline SBF', is shown in Fig.4. For the references, the spectra of the Sample N, Sample S and Sample SP are also shown. Before the 'Alkaline SBF' treatment, the FT-IR spectrum was almost same as the untreated substrates even after the $H_2SO_4$ treatment and the $O_2$ plasma treatment. After the 'Alkaline SBF' treatment, however, absorption peaks attributed to P=O bonds which characterize the existence of $PO_4^{3-}$ group were clearly observed around 1000 $cm^{-1}$. From the FT-IR results, it is considered that some kinds of phosphate salts were newly generated by the 'Alkaline SBF' treatment. In the Miyazaki's study [29], peaks of O=S=O were observed at 1050 $cm^{-1}$ and 1200 $cm^{-1}$ after $H_2SO_4$ treatment for 10 minutes. However, our study did not show such peaks in the FT-IR measurement. Similar to the EDX result, it is considered that this difference was caused by a time of the $H_2SO_4$ treatment.

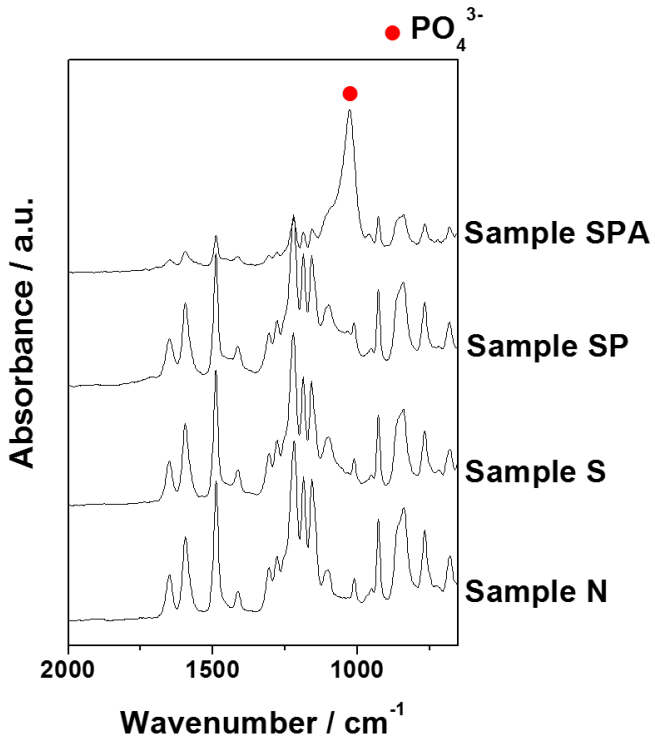


Fig.4 FT-IR spectra of the surface of Sample N, Sample S, Sample SP and Sample SPA.

The FE-SEM photograph and the EDX spectrum of the surface of Sample SPA are shown in Fig.5. In comparison with Sample SP, it was revealed that the spherical particles with ca. 100 nm in diameter were uniformly observed on the whole surface of the substrate after the 'Alkaline SBF' treatment as shown in Fig.5(a). In addition, a peak of Ca-Kα was clearly observed in the EDX as shown in Fig.5(b). Taking into consideration the results of the FT-IR, FE-SEM and EDX, it is considered that the fine particles of calcium phosphate were formed by the 'Alkaline SBF' treatment.

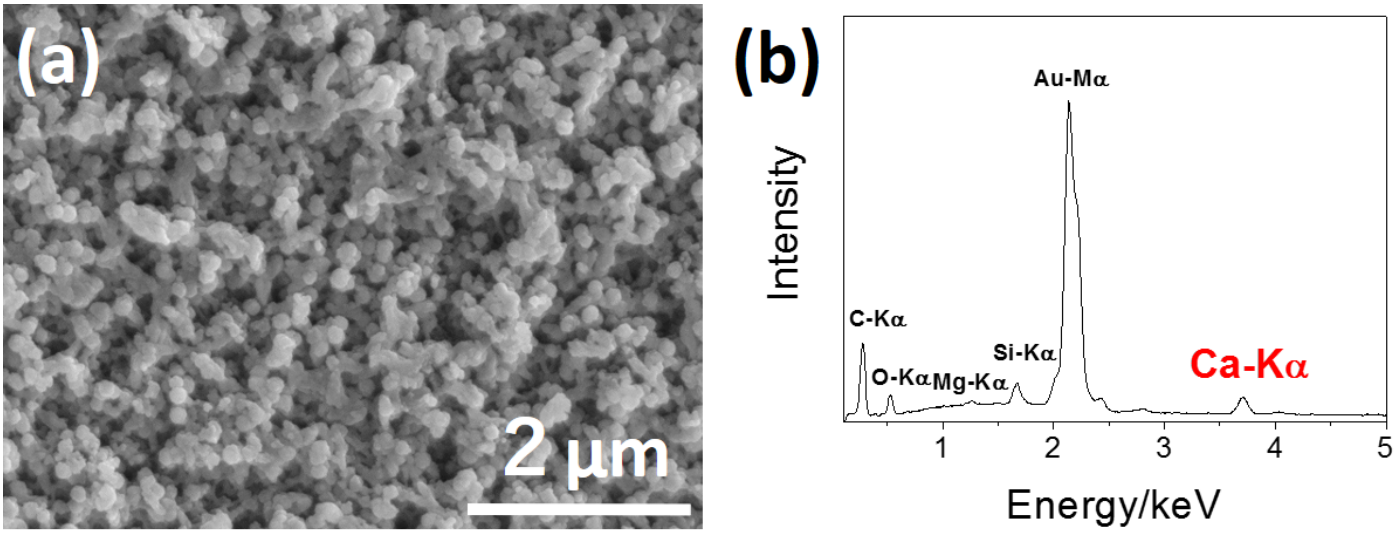


Fig. 5 (a) FE-SEM photograph and (b) EDX spectrum of the surface of Sample SPA.

The TF-XRD patterns of the surface of the Sample SPA is shown in Fig.6. For the references, patterns of Sample N, Sample S and Sample SP are also shown. Although fine particles of calcium phosphate were observed on the surface after the 'Alkaline SBF' treatment as shown in Fig.4 and Fig.5, diffraction peaks of hydroxyapatite were not observed even after the 'Alkaline SBF' treatment. Taking into consideration the results of the FT-IR, FE-SEM, EDX and TF-XRD, it is considered that the fine particles formed by the 'Alkaline SBF' treatment were constructed of amorphous calcium phosphate.

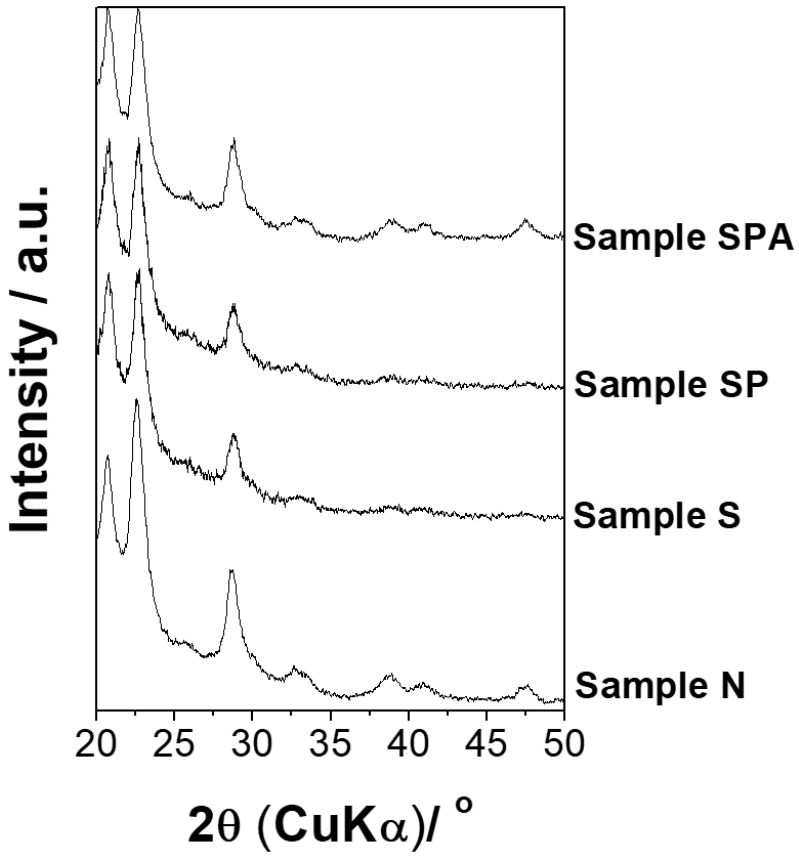


Fig.6 TF-XRD patterns of the surface of Sample N, Sample S, Sample SP and Sample SPA.

Generally, hydroxyapatite formation in an aqueous solution can be described as shown in below.

$$10Ca^{2+} + 6PO_4^{3-} + 2OH^- \leftrightarrow Ca_{10}(PO_4)_6(OH)_2$$

When the pH value of the aqueous solution increases, hydroxyapatite formation is progressed from the view point of a chemical equilibration because of an increase of $OH^-$. In this study, the reaction was accelerated by the high temperature environment (70.0 °C) in comparison with the physiological

temperature (36.5 °C). In the case of SBF, the aqueous solution contains several kinds of additional ions such as $Na^+$, $Mg^{2+}$, $K^+$, $Cl^-$ and $HCO_3^-$ beside $Ca^{2+}$ and $PO_4^{3-}$ or $HPO_4^{2-}$ as shown in Table 1. Hence, it is considered that a crystallization of the deposited calcium phosphate was inhibited by an existence of these additional ions in the 'Alkaline SBF' treatment. As a result, the formed calcium phosphate possessed the amorphous phase rather than crystal phase such as hydroxyapatite. In this report, the authors define these fine particles of amorphous calcium phosphate as 'PrA', hereafter.

### 3.1.3. Hydroxyapatite formation ability

The FT-IR spectra of the surfaces of Sample SPA before and after the immersion in SBF for 1 day, 4 days, 7 days and 14 days are shown in Fig.7(a). Absorption peaks attributed to P=O bonds, which characterize the existence of $PO_4^{3-}$ group, were observed around 1000 $cm^{-1}$ both before and after the immersion in SBF for each period. In addition, peaks derived from the untreated PEEK was almost disappeared after the immersion in SBF. It is suggested that the PrA formed calcium phosphate layers in SBF and the PEEK substrates became unexposed by the layers.

The TF-XRD patterns of the surface of Sample SPA before and after the immersion in SBF for 1 day, 4 days, 7 days and 14 days are shown in Fig.7(b). After the immersion in SBF for 1 day, broad diffraction peaks of hydroxyapatite were slightly observed around $2\theta=26°$ and 31°. As increasing the immersion period, the intensity of and the number of diffraction peaks of hydroxyapatite increased and the patterns of the PEEK substrate decreased. From the TF-XRD results, it is considered that the PrA, constructed of amorphous phase, grew into crystalline hydroxyapatite by the immersion in SBF.

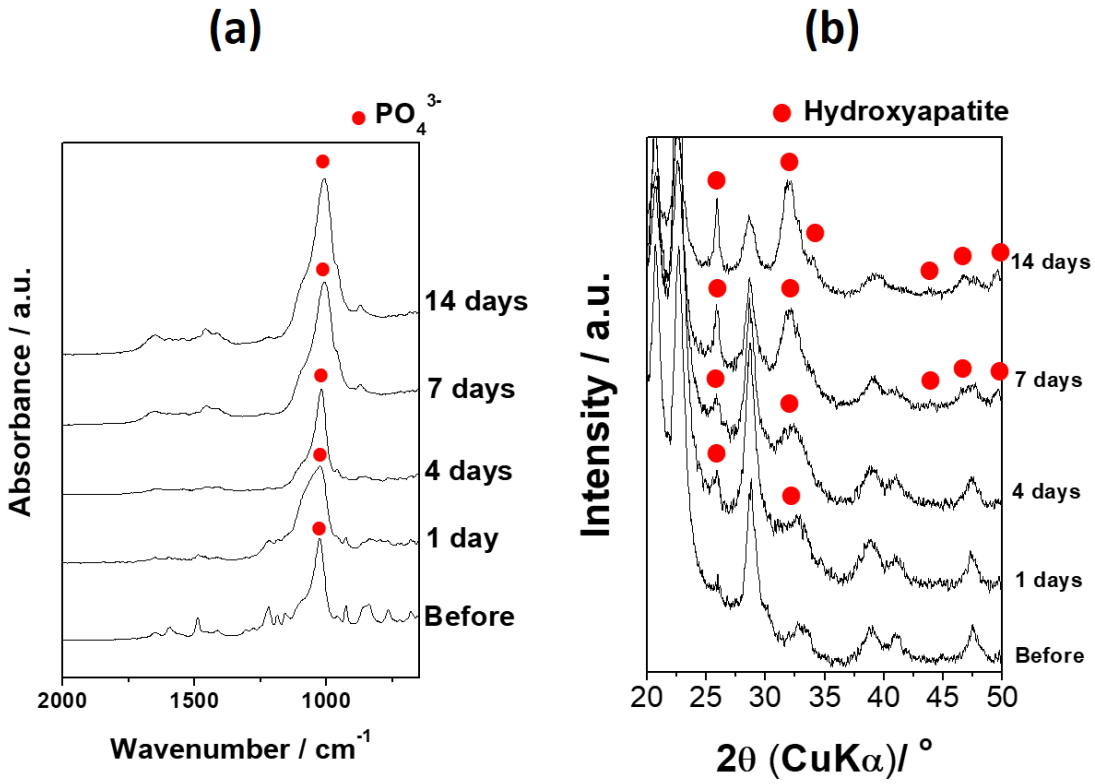


Fig.7 (a) FT-IR spectra and (b) TF-XRD patterns of the surface of Sample SPA before and after the immersion in SBF for 1 day, 4 days, 7 days and 14 days.

The FE-SEM photograph and the EDX spectrum of the surfaces of the Sample SPA after the immersion in SBF for 1 day are shown in Figs.8(a) and 8(b). After the immersion in SBF for each period, the whole surface was covered with flake-like crystallites, which characterize hydroxyapatite formed in SBF, as shown in Fig.8(a). By the EDX, peaks of P-Kα, Ca-Kα and Ca-Kβ were clearly observed in comparison with before the immersion in SBF shown in Fig.8(b). In addition, a small amount of Na-Kα and Mg-Kα were observed, similar to the Takadama's result on hydroxyapatite layers formed in SBF on bioactive titanium [32,40]. These characteristics are similar to those of bone mineral. Okazaki et al. reported that hydroxyapatite which contained Mg in Ca sites showed low crystallinity in comparison with stoichiometric hydroxyapatite [41]. Taking into consideration the results of the EDX and the TF-XRD, it is suggested that the additional Mg and Na ions were incorporated in crystal structure of the hydroxyapatite and the low crystallinity was obtained as shown in Fig.7(b).

Taking into consideration the results of the FT-IR, TF-XRD, FE-SEM and EDX, it is revealed that the hydroxyapatite formation was induced by the PrA in SBF and the hydroxyapatite covered the

whole surface of the substrate within 1 day. From these results, it is shown that high hydroxyapatite formation ability was performed on the PEEK substrate by conducting the series of each treatment.

Zhao et al. reported that PEEK substrate treated with $H_2SO_4$ showed hydroxyapatite formation within 28 days in SBF [30]. In addition, Miyazaki et al. reported that PEEK treated with $H_2SO_4$ and subsequently treated with $CaCl_2$ was showed hydroxyapatite formation within 14 days in SBF [29]. From a viewpoint of induction period of hydroxyapatite formation in SBF, this result suggests that the 'Alkaline SBF' treatment in this study is effective for promotion of the hydroxyapatite formation. In addition, it was reported that most of bioactive materials for orthopedic application form apatite within 1 week [16]. From this point, it is considered that the 'Alkaline SBF' treatment in this study is a candidate as a promising process to provide bioactivity to PEEK.

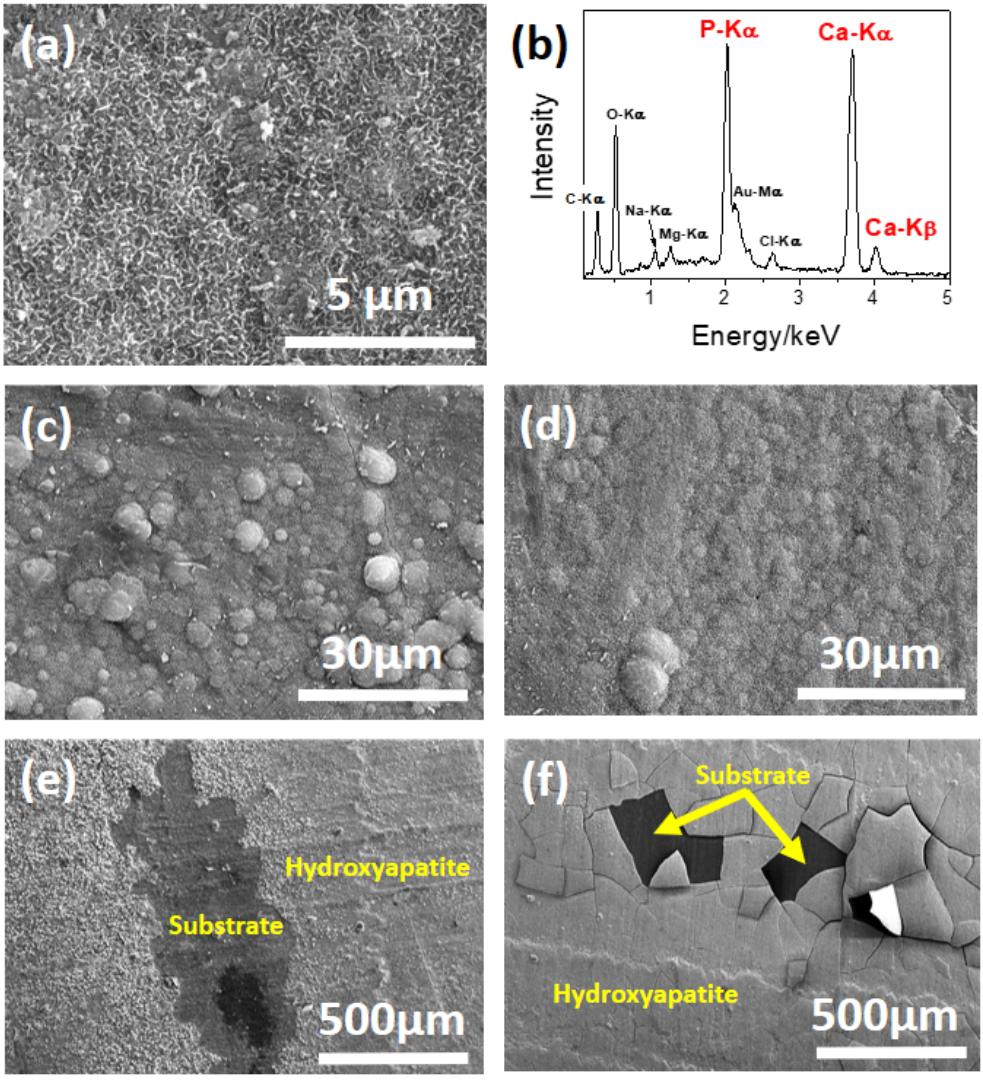


Fig.8 (a) FE-SEM photograph and (b) EDX spectrum of the surface of Sample SPA after the immersion in SBF for 1 day, and FE-SEM photographs after the immersion in SBF for 7 days for the surface of (c) Sample SPA, (d) Sample PA, (e) Sample SA and (f) Sample A.

### 3.1.4. Effect of 'Alkaline SBF' treatment to hydroxyapatite formation

On Samples SP, Sample S, Sample P and Sample N, without 'Alkaline SBF' treatment, no hydroxyapatite was formed after the immersion in SBF for 7 days. On Sample SPA, Sample SA and Sample A, with 'Alkaline SBF' treatment, by contrast, hydroxyapatite formation was observed after the immersion in SBF for 7 days. It was revealed that the 'Alkaline SBF' treatment was essential process to provide hydroxyapatite formation ability to the PEEK substrate.

### 3.1.5. Effect of $O_2$ plasma treatment to hydroxyapatite formation

Figs.8(c), 8(d), 8(e) and 8(f) shows the FE-SEM photographs of the surfaces of Sample SPA, Sample PA, Sample SA and Sample A after the immersion in SBF for 7 days. As shown in Figs.8(c) and 8(d), Sample SPA and Sample PA was covered the whole surfaces with hydroxyapatite by the immersion in SBF. As shown in Figs.8(e) and 8(f), by contrast, hydroxyapatite formation on Sample SA and Sample A was not sufficient. In the case of Sample SA, hydroxyapatite was partially covered with hydroxyapatite even after the immersion in SBF for 7 days as shown in Fig.8(e). It is suggested that the $O_2$ plasma treatment was necessary to form the hydroxyapatite on the whole surfaces of the PEEK substrates because hydrophilic properties were provided and the 'Alkaline SBF' was uniformly penetrated in the pores on the whole surface during the formation process of PrA. In the case of Sample A, the formed hydroxyapatite layer was easily peeled off as shown in Fig.8(f). It is suggested that the $O_2$ plasma treatment also contributed to improve the adhesive strength between the hydroxyapatite layer and the PEEK substrate.

### 3.1.6. Effect of $H_2SO_4$ treatment to hydroxyapatite formation

Fig.9 shows average adhesive strengths between the PEEK substrate and the hydroxyapatite layer formed on Sample SPA and Sample PA by the immersion in SBF for 14 days. In Fig.9, error bars show standard deviations. The average adhesive strengths and standard deviations were 6.67 (1.51) MPa for 12 substrates for Sample SPA and 2.10 (0.83) MPa for 8 substrates for Sample PA, respectively. In the FE-SEM observation, there was not clear difference on coating areas of the formed hydroxyapatite layer as shown in Fig.8(c) and Fig.8(d). However, a considerable difference

on the adhesive strength of hydroxyapatite layer were found out. The Sample SPA realized almost three times of the adhesive strength in comparison with the Sample PA. This is because the hydroxyapatite layer behaves as an anchor in the pores of the PEEK substrate. As shown in Fig.1(c), cancellous pores were formed by the $H_2SO_4$ treatment. As shown in Fig.3, moreover, the $H_2SO_4$ treatment causes the increase of the surface area. From these results, it is suggested that the increase of the surface area effectively attributed to a mechanical anchoring effect from the viewpoint of the adhesion of the hydroxyapatite layer on this material.

Considering clinical applications, the important limitation of Method 1 is located on the relationship between hydroxyapatite formation inside the pores and the mechanical anchoring effect. It is speculated that the mechanical anchoring effect is effectively achieved when the hydroxyapatite is deeply formed inside the pores. To explain this point clearly, it is thought that cross-sectional observations of the substrate is essential before and after the immersion in SBF. If the formed hydroxyapatite is tightly meshed inside the pores, suppressions of bacterial growth at the interface on the substrate as well as strong mechanical anchoring effects is expected. This point will be examined in a future study.

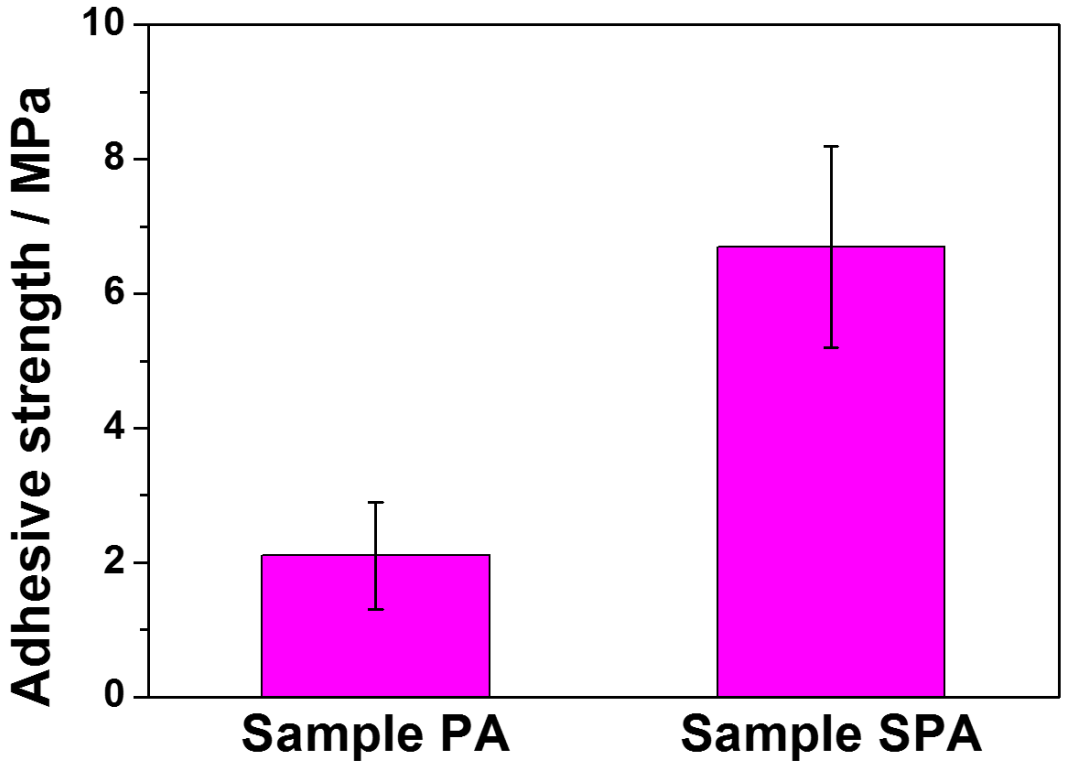


Fig.9 Average adhesive strength between PEEK substrate and hydroxyapatite layer formed on Sample PA and Sample SPA by immersion in SBF for 14 days.

### 3.2. Method 2: Employment of sandblasting method as pores formation

The FE-SEM photographs and the EDX spectra of the surfaces of Sample 44, Sample 13 and Sample 44-13 are shown in Figs.10(a), 10(b) and 10(c). Although gentle rolling was observed on each substrate, pores with fine size like the case of the $H_2SO_4$ treatment was not observed. In the EDX, in addition, peaks of Al-Kα was clearly observed on each substrate. The existence of this peak means that the alumina grinding particles were remained on the substrate even after the washing by using ultrasonic cleaner.

The FE-SEM photographs and the EDX spectra of the surfaces of Sample 44PA, Sample 13PA and Sample 44-13PA after the immersion in SBF for 7 days are shown in Figs.10(d), 10(e) and 10(f). After the immersion in SBF for 7 days, flake-like crystallites, which characterize hydroxyapatite formed in SBF, were observed. By the EDX, peaks of P-Kα, Ca-Kα and Ca-Kβ were observed. This result means that Sample 44PA, 13PA and 44-13PA possessed hydroxyapatite formation ability.

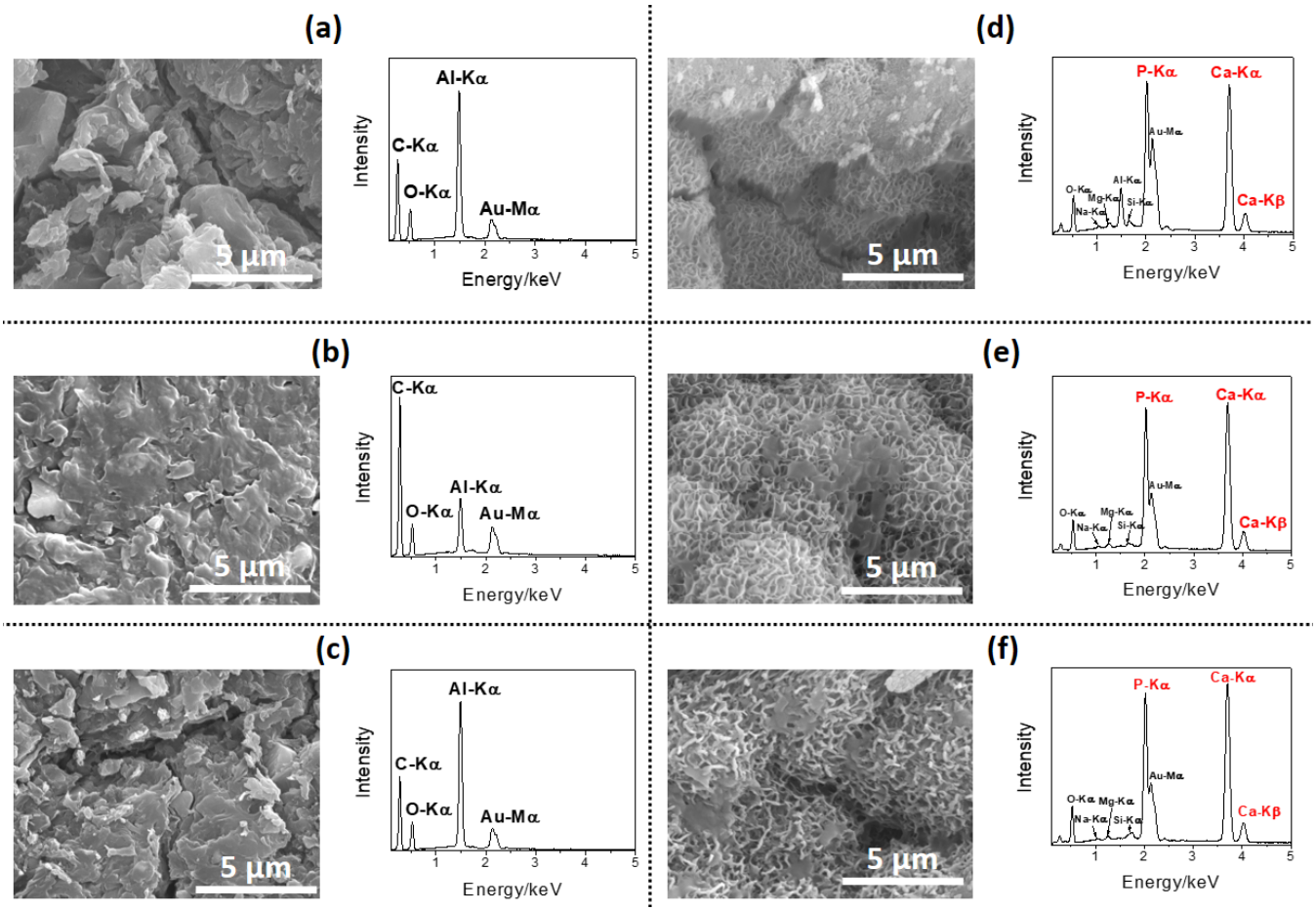


Fig.10 FE-SEM photographs and EDX spectra of (a) 44P, (b) 13P, (c) 44-13P, (d) 44PA after the immersion in SBF for 7 days, (e) 13PA after the immersion in SBF for 7 days, and (f) 44-13PA after the immersion in SBF for 7 days.

Although hydroxyapatite formation was achieved on Sample 44PA, 13PA and 44-13PA as shown in Figs.10(d), 10(e) and 10(f), however, adhesive strength between hydroxyapatite layers and these samples was not able to be measured because the hydroxyapatite layers were easily peeled off before the measurements. Compared with the result of Sample PA, only treated with $O_2$ plasma, shown in Fig.8(d), the result of Method 2 was contrary to the expectation. It is speculated that this perverse result is because unsuitable shapes of pores obtained by the sandblasting process caused a formation of gaps between the hydroxyapatite layer and the substrate. By using the sandblasting methods, pores of fine structures were not formed as shown in Fig.10(a), 10(b) and 10(c). Hence, the mechanical anchoring effect was not achieved in comparison with the $H_2SO_4$ treatment and the hydroxyapatite layer was weakly adhered even if the $O_2$ plasma treatment was conducted.

The limitation of Method 2 is located on choices of the grinding particles. Generally, pores formation by the sandblasting method are impacted by sizes and kinds of grinding particles depending on kinds of the substrates. In fact, the authors reported that the doubled sandblasting process using different sizes of ceramic grinding particles was available to enhancement of adhesive strength of hydroxyapatite layer coated on titanium alloys [42]. Hence, it may be possible to form a suitable size of pores by investigation of suitable grinding particles on the sandblasting method. This point will be examined in a future study.

## 4. Conclusion

The authors successfully prepared bioactive PEEK by forming cancellous fine pores on the surface of the PEEK by the $H_2SO_4$ treatment, conducting $O_2$ plasma treatment and depositing PrA in the pores. By the immersion in SBF, it was observed that the whole surface of thus fabricated bioactive PEEK was covered with hydroxyapatite within 1 day. The formed hydroxyapatite layer showed high adhesive strength to the PEEK substrate by the mechanical anchoring effect. The pores formation by the $H_2SO_4$ treatment was much more effective to obtain high adhesive strength of the hydroxyapatite layer than that by the sandblasting method. This material is promising as attractive implant materials with high bioactivity as well as good mechanical performance for clinical applications.

**Acknowledgment**

This work was partly supported by JSPS KAKENHI Grant Number JP16K16401 and Kyoto University Research Development Program “Ishizue”.

**References**

[1] L.L. Hench, R.J. Splinter, W.C. Allen, T.K. Greenlee Jr., Bonding mechanism at the influence of ceramics prosthetic materials, J. Biomed. Mater. Res. Symp. 2 (1972) 117-141.

[2] L.L. Hench, Bioceramics: from concept to clinic, J. Biomed. Mater. Res. 74 (1991) 1487-1510.

[3] L.L. Hench, Örjan Andersson, Bioactive glasses, in: L.L. Hench, J. Wilson (Eds.), An Introduction to Bioceramics, World Scientific Publishing Co. Pte. Ltd., Singapore, 1993, pp. 41-62.

[4] U.M. Gross, C. Müller-Mai, C. Voigt, Ceravital® bioactive ceramics, in: L.L. Hench, J. Wilson (Eds.), An Introduction to Bioceramics, World Scientific Publishing Co. Pte. Ltd., Singapore, 1993, pp. 105-124.

[5] T. Kokubo, M. Shigematsu, Y. Nagashima, M. Tashiro, T. Yamamuro, S. Higashi, Apatite- and wollastonite-containing glass-ceramics for prosthetic application, Bull. Inst. Chem. Res. Kyoto Univ., 60 (1982) 260-268.

[6] T. Kokubo, A/W glass-ceramic: processing and properties, in: L.L. Hench, J. Wilson (Eds.), An Introduction to Bioceramics, World Scientific Publishing Co. Pte. Ltd., Singapore, 1993, pp. 75-88.

[7] T. Kokubo, Bioactive glass-ceramics, in: T. Kokubo (Ed.), Bioceramics and their clinical applications, Woodhead Publishing Limited, Cambridge, 2008, pp.284-301.

[8] M. Jarcho, J.L. Kay, R.H. Gumaer, H.P. Drobeck, Tissue, cellular and subcellular events at bone-ceramic hydroxyapatite interface, J. Bioeng., 1 (1977) 79-92.

[9] H. Aoki, K. Kato, M. Ogiso, T. Tabata, Sintered hydroxyapatite as a new dental implant material, J. Dent. Outlook, 49 (1977) 567-575.

[10] R.Z. LeGeros and J.P. LeGeros, Dense hydroxyapatite, in: L.L. Hench, J. Wilson (Eds.), An Introduction to Bioceramics, World Scientific Publishing Co. Pte. Ltd., Singapore, 1993, pp. 139-180.

[11] R.Z. LeGeros and J.P. LeGeros, Hydroxyapatite, in: T. Kokubo (Ed.), Bioceramics and their clinical applications, Woodhead Publishing Limited, Cambridge, 2008, pp.367-394.

[12] M. Neo, S. Kotani, Y. Fujita, T. Nakamura, T. Yamamuro, Y. Bando, C. Ohtsuki, T. Kokubo, Differences in ceramics-bone interface between surface-active ceramics and resorbable ceramics: a study by scanning and transmission electron microscopy, J. Biomed. Mater. Res., 26 (1992) 255-267.

[13] M. Neo, T. Nakamura, C. Ohtsuki, T. Kokubo, T. Yamamuro, Apatite formation on three kinds of bioactive material at an early stage in vivo: a comparative study by transmission electron microscopy, J. Biomed. Mater. Res. 27 (1993) 999-1006.

[14] P. Virolainen, J. Heikkila, A. Yli-Urpo, E. Vuorio, H.T. Aro, Histommorphometric and molecular biologic comparison of bioactive glass granules and autogenous bone grafts in augmentation of bone defect healing, J. Biomed. Mater. Res. 35 (1997) 9-17.

[15] T. Kokubo, H. Kushitani, S. Sakka, T. Kitsugi, T. Yamamuro, Solutions able to reproduce in vivo surface-structure changes in bioactive glass-ceramics, J. Biomed. Mater. Res., 24 (1990) 721-724.

[16] T. Kokubo, H. Takadama, How useful is SBF in predicting in vivo bone bioactivity?, Biomaterials, 27 (2006) 2907-2915.

[17] H. Takadama, T. Kokubo, In vitro evaluation of bone bioactivity, in: T. Kokubo (Ed.), Bioceramics and their clinical applications, Woodhead Publishing Limited, Cambridge, 2008, pp.165-182.

[18] ISO 23317, Implants for surgery - In vitro evaluation for apatite-forming ability of implant materials, International Organization for Standardization (2014).

[19] S.M. Kurtz, J.N. Devine, PEEK biomaterials in trauma, orthopedic, and spinal implants, Biomaterials, 28 (2007) 4845-4869.

[20] M. Niinomi, Development of titanium alloys with high mechanical biocompatibility with focusing on controlling elastic modulus, Materia Japan, 52 (2013) 219-228.

[21] W. Bonfield, M.D. Grynpas, A.E. Tully, J. Bowman, J. Abram, Hydroxyapatite reinforced polyethylene--a mechanically compatible implant material for bone replacement, Biomaterials (1981) 185-186.

[22] W. Bonfield, Design of bioactive ceramics-polymer composites, in: L.L. Hench, J. Wilson (Eds.), An Introduction to Bioceramics, World Scientific Publishing Co. Pte. Ltd., Singapore, 1993, pp. 299-303.

[23] C. Ohtsuki, Bioactive composite materials, J. Adhes. Soc. Japan 39 (2003) 125-130.

[24] R. Ma, T. Tang, Current strategies to improve the bioactivity of PEEK, Int. J. Mol. Sci. 15 (2014) 5426-5445.

[25] M.S. Abu Bakar, P. Cheang, K.A. Khor, Mechanical properties of injection molded hydroxyapatite-polyetheretherketone biocomposites, Combust. Sci. Technol. 63 (2003) 421–425.

[26] J.P. Fan, C.P. Tsui, C.Y. Tang, C.L. Chow, Influence of interphase layer on the overall elasto-plastic behaviors of HA/PEEK biocomposite, Biomaterials 25 (2004) 5363–5373.

[27] B. Yuan, Y. Chen, H. Lin, Y. Song, X. Yang, H. Tang, E. Xie, T. Hsu, X. Yang, X. Zhu, K. Zhang, X. ZhangProcessing and properties of bioactive surface-porous PEKK, ACS Biomater. Sci. Eng. 2 (2016) 977–986

[28] I.Y. Kim, A. Sugino, K. Kikuta, C. Ohtsuki, S.B. Cho, Bioactive composites consisting of PEEK and calcium silicate powders, J. Biomater. Appl., 24 (2009) 105–118.

[29] T. Miyazaki, C. Matsunami, Y. Shirosaki, Bioactive carbon–PEEK composites prepared by chemical surface treatment, Mater. Sci. Eng. C 70 (2017) 71-75.

[30] Y. Zhao, H.M. Wong, W. Wang, P. Li, Z. Xu, E.Y.W. Chong, C.H. Yan, K.W.K. Yeung, P.K. Chu, Cytocompatibility, osseointegration, and bioactivity of three-dimensional porous and nanostructured network on polyetheretherketone, Biomaterials 34 (2013) 9264–9277.

[31] T. Shimizu, S. Fujibayashi, S. Yamaguchi, K. Yamamoto, B. Otsuki, M. Takemoto, M. Tsukanaka, T. Kizuki, T. Matsushita, T. Kokubo, S. Matsuda, Bioactivity of sol–gel-derived $TiO_2$ coating on polyetheretherketone: In vitro and in vivo studies, Acta Biomaterialia 35 (2016) 305-317.

[32] T. Kokubo, H. Takadama, T. Matsushita, Titania-based materials, in: T. Kokubo (Ed.), Bioceramics and their clinical applications, Woodhead Publishing Limited, Cambridge, 2008, pp.485-500.

[33] T. Yao, M. Hibino, T. Yabutsuka, Method for producing bioactive composites, U.S. Patent (2013) 8512732, Japanese Patent (2013) 5252399.

[34] T. Yao, M. Hibino, S. Yamaguchi, H. Okada, Method for stabilizing calcium phosphate fine particles, process for production of calcium phosphate fine particles by utilizing the method, and use thereof, U.S. Patent (2012) 8178066, Japanese Patent (2013) 5261712.

[35] M. Tanahashi, T. Yao, T. Kokubo, M. Minoda, T. Miyamoto, T. Nakamura, T. Yamamuro, Apatite coated on organic polymers by biomimetic process: Improvement in its adhesion to substrate by glow-discharge treatment, J. Biomed. Mater. Res. 29 (1995) 349-357.

[36] W.R. Lacefield, Hydroxylapatite coatings, in: L.L. Hench, J. Wilson (Eds.), An Introduction to Bioceramics, World Scientific Publishing Co. Pte. Ltd., Singapore, 1993, pp. 223-238.

[37] Designation C-633, Annual Book of ASTM Standards, Vol. 3.01, American Society for Testing and Materials (1993) pp. 665-699.

[38] J.A. Juhasz, S.M. Best, M. Kawashita, N. Miyata, T. Kokubo, T. Nakamura, W. Bonfield, Bonding strength of the apatite layer formed on glass-ceramic apatite-wollastonite–polyethylene composites, J. Biomed. Mater. Res. Part A (2003) 952-959.

[39] T. Yao, T. Yabutsuka, Material having pores on surface, and method for manufacturing same, Japanese Patent (2017) 6071895.

[40] H. Takadama, H.-M. Kim, T. Kokubo, T. Nakamura, TEM-EDS study of mechanism of bonelike apatite formation on bioactive titanium metal in simulated body fluid, J. Biomed. Mater. Res. 57 (2001) 441-448.

[41] M. Okazaki, J. Takahashi, H. Kimura, Unstable behavior of magnesium-containg hydroxyapatites, Caries Res., 20 (1986) 324-331.

[42] T. Yabutsuka, H. Mizuno, R. Karashima, T. Yao, Fabrication of bioactive apatite nuclei precipitated Ti-15Mo-5Zr-3Al alloy by using doubled sandblasting process, Key Eng. Mater. 631 (2015) 231-235.